

Effective spin physics in two-dimensional cavity QED arrays

This content has been downloaded from IOPscience. Please scroll down to see the full text.

2017 New J. Phys. 19 063033

(<http://iopscience.iop.org/1367-2630/19/6/063033>)

View [the table of contents for this issue](#), or go to the [journal homepage](#) for more

Download details:

IP Address: 128.243.2.47

This content was downloaded on 03/08/2017 at 11:23

Please note that [terms and conditions apply](#).

You may also be interested in:

[Non-equilibrium dynamics of a nonlinear Jaynes–Cummings model in cavity arrays](#)

Jiří Minář, Ebnem Güne Söyler and Igor Lesanovsky

[Quantum phase transitions in the collective degrees of freedom: nuclei and other many-body systems](#)

Pavel Cejnar and Pavel Stránský

[Keldysh field theory for driven open quantum systems](#)

L M Sieberer, M Buchhold and S Diehl

[Quantum simulation with interacting photons](#)

Michael J Hartmann

[Experimental investigations of dipole–dipole interactions between a few Rydberg atoms](#)

Antoine Browaeys, Daniel Barredo and Thierry Lahaye

[S-matrices and Integrability](#)

Diego Bombardelli

[Field-dependent superradiant quantum phase transition of molecular magnets in microwave cavities](#)

Dimitrije Stepanenko, Mircea Trif, Oleksandr Tsyplatyev et al.

[The field treatment of the nuclear spectrum. Historical foundation and two contributions to its ensuing development](#)

Daniel R Bes

[A coordinate Bethe ansatz approach to the calculation of equilibrium and nonequilibrium correlations of the one-dimensional Bose gas](#)

Jan C Zill, Tod M Wright, Karén V Kheruntsyan et al.



PAPER

Effective spin physics in two-dimensional cavity QED arrays

Jiří Minář^{1,2,3}, Şebnem Güneş Söyler^{1,2}, Pietro Rotondo^{1,2} and Igor Lesanovsky^{1,2}¹ School of Physics and Astronomy, The University of Nottingham, Nottingham, NG7 2RD, United Kingdom² Centre for the Theoretical Physics and Mathematics of Quantum Non-equilibrium Systems, The University of Nottingham, Nottingham, NG7 2RD, United Kingdom³ Author to whom any correspondence should be addressedE-mail: minarjiri@gmail.com**Keywords:** cavity arrays, ground states of spin systems, frustrated spin models, quantum Monte Carlo, Dicke, Jaynes–Cummings, Tavis–Cummings modelsRECEIVED
9 February 2017REVISED
18 May 2017ACCEPTED FOR PUBLICATION
26 May 2017PUBLISHED
3 July 2017

Original content from this work may be used under the terms of the [Creative Commons Attribution 3.0 licence](#).

Any further distribution of this work must maintain attribution to the author(s) and the title of the work, journal citation and DOI.

**Abstract**

We investigate a strongly correlated system of light and matter in two-dimensional cavity arrays. We formulate a multimode Tavis–Cummings (TC) Hamiltonian for two-level atoms coupled to cavity modes and driven by an external laser field which reduces to an effective spin Hamiltonian in the dispersive regime. In one-dimension we provide an exact analytical solution. In two-dimensions, we perform mean-field study and large scale quantum Monte Carlo simulations of both the TC and the effective spin models. We discuss the phase diagram and the parameter regime which gives rise to frustrated interactions between the spins. We provide a quantitative description of the phase transitions and correlation properties featured by the system and we discuss graph-theoretical properties of the ground states in terms of graph colourings using Pólya’s enumeration theorem.

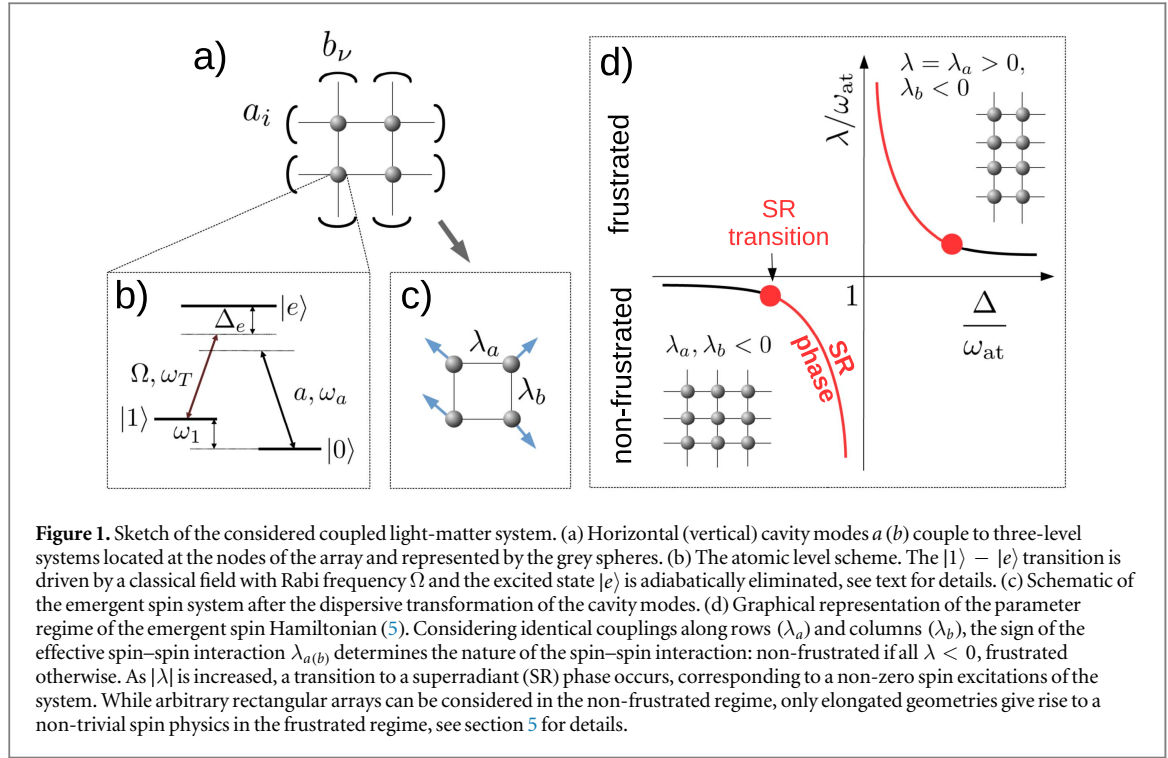
1. Introduction

Strongly coupled light-matter systems are at the heart of much of the effort in modern atomic and optical physics with applications ranging from quantum information processing to quantum simulations.

In this context, the use of cavities plays a prominent role as the strong confinement of the electromagnetic field implies strong interaction with matter coupled to the cavity modes. In particular, it offers possibilities to realize and study a plethora of quantum light-matter many-body Hamiltonians such as the so-called Jaynes–Cummings–Hubbard or Rabi–Hubbard models [1–11], or quantum fluids of light, where the effective interaction between light fields is mediated by a nonlinear medium [12–14]. This offers ways to study various physical phenomena such as excitation propagation in chiral networks [15–17], the physics of spin glasses [18–20] and quantum Hopfield networks [21, 22], self-organization of the atomic motion in optical cavities [23–27] or quantum phase transitions in arrays of nanocavity quantum dots [28] and in Coulomb crystals [29]. Furthermore, modern implementations of optical and microwave cavities allow for the creation of lattices with tunable geometries and dimensionality [30–32].

The paradigmatic description of cavity and circuit QED systems is typically in terms of the famous Dicke [33], Jaynes–Cummings [34] or Tavis–Cummings (TC) [35, 36] models, which describe the interaction between the modes of the light field and the matter constituents, typically spin or phononic degrees of freedom of atoms or ions. Importantly, effective spin models emerge in the dispersive limit of the TC or Dicke models [37, 38]. Under some circumstances this leads to spin Hamiltonians with frustrated or long-range interactions [19, 39, 40], thus offering ways to study rich physics of quantum magnetism. This is a particularly interesting direction allowing e.g. for studies of spin liquids [41–43] with optical quantum simulators.

While advanced numerical techniques, such as tensor networks, have been developed for spin Hamiltonians [44–47], the use of similarly efficient techniques for quantum optical systems, where a system of spins is coupled to the bosonic modes of an electromagnetic field remains limited. In this work we use mean-field (MF) description, exact diagonalization and large-scale quantum Monte Carlo (QMC) algorithm to study arrays of waveguide cavities (we note that in the context of cavity QED, QMC was implemented to study both the



Jaynes–Cummings–Hubbard [48] and the Rabi–Hubbard [49] models). This gives us rigorous tools to investigate the emergence of the effective spin physics as a limiting case of the parent TC Hamiltonian for arbitrary lattice geometries and dimensions. Specifically, in this work we focus on square lattice geometry and we study the ground state properties of the TC and the effective spin models for various parameter regimes. We then show, that depending on the parameter regime and the array geometry, spin models with both non-frustrated and frustrated interactions can be engineered.

The paper is organized as follows. In section 2 we introduce the system and derive the effective spin model from the parent TC Hamiltonian. In section 3 we present exact analytical solution of the spin model in one-dimension. In section 4 we present the results of the QMC simulation and MF analysis and discuss different regimes provided by the investigated model. We explain how the present work opens possibilities for simulating frustrated systems in section 5 and conclude in section 6.

2. Effective Hamiltonians

2.1. Multimode TC Hamiltonian

Recent advances in integrated optical circuits, where in principle arbitrary waveguide geometries can be created with high precision by laser engraving in the silica substrate [50] and an active experimental effort to combine the waveguides with atomic microtraps on a single device [51, 52] motivate us to investigate a system of three-level atoms embedded in waveguide cavities.

We consider a square cavity array, where we denote by a_i (b_ν) the modes in the i th row (ν th column) of the array, as shown in figure 1(a). We use the latin (greek) indices to denote the rows (columns) throughout the article. All sites of the array are occupied by identical three-level systems in a Λ configuration, where $|0\rangle$, $|1\rangle$ denote the ground states and $|e\rangle$ the excited state, see figure 1(b). The cavity modes are coupled with strength g_0 to the $|0\rangle - |e\rangle$ transition, while the $|1\rangle - |e\rangle$ transition couples to a classical field Ω with frequency ω_T which propagates perpendicularly to the plane of the array and which is detuned by $\Delta_e = \omega_1 - \omega_T$ with respect to the $|1\rangle - |e\rangle$ transition. In the limit $\Delta_e \gg g_0$, Ω one can eliminate the excited state, which we described in detail in our previous publication [53]. Furthermore, under the condition of strong driving

$$\Omega \gg g_0 \quad (1)$$

the resulting Hamiltonian is of the TC type and reads (see appendix A for the details of the derivation and of the full Hamiltonian)

$$H_{\text{TC}} = \sum_i \Delta_i a_i^\dagger a_i + \sum_\nu \Delta_\nu b_\nu^\dagger b_\nu + \frac{\omega_{\text{at}}}{2} \sum_{i,\nu} \sigma_{i\nu}^z + g \sum_{i,\nu} (\sigma_{i\nu}^+ a_i + a_i^\dagger \sigma_{i\nu}^-) + g \sum_{i,\nu} (\sigma_{i\nu}^+ b_\nu + b_\nu^\dagger \sigma_{i\nu}^-). \quad (2)$$

with the effective atomic transition frequency and the effective coupling strength

$$\omega_{\text{at}} = -\frac{\Omega^2}{\Delta_e}, \quad (3a)$$

$$g = -\frac{g_0 \Omega}{\Delta_e}. \quad (3b)$$

Here, $\sigma_{i\nu}^{z,\pm}$ are the usual Pauli matrices written in the $\{|1\rangle, |0\rangle\}$ basis, $\Delta_{i(\nu)}$ the effective cavity frequencies, ω_{at} the effective frequency of the $|0\rangle - |1\rangle$ transition and $i = 1 \dots L_y$, $\nu = 1 \dots L_x$, where L_y (L_x) is the number of rows (columns) of the array.

2.2. Spin Hamiltonian

In the large detuning (dispersive) limit

$$g \ll |\omega_{\text{at}} - \Delta_{i(\nu)}|, \quad (4)$$

one can further perform a unitary transformation to perturbatively eliminate the cavity fields in order to obtain an effective spin Hamiltonian, where a given spin is coupled to all other spins belonging to the same cavity mode (see figure 1(c) and appendix A),

$$H_{\text{spin}} = H_{\text{spin},0} + \delta H + H_{\text{spin,int}}, \quad (5)$$

where

$$H_{\text{spin},0} = \sum_{i,\nu} \left(\frac{\omega_{\text{at}}}{2} + \lambda_i + \lambda_\nu \right) \sigma_{i\nu}^z, \quad (6a)$$

$$\delta H = \sum_{i,\nu} \delta \omega_{\text{at},i\nu} \sigma_{i\nu}^z, \quad (6b)$$

$$H_{\text{spin,int}} = \sum_{i,\nu \neq \mu} \lambda_i (\sigma_{i\nu}^- \sigma_{i\mu}^+ + \sigma_{i\nu}^+ \sigma_{i\mu}^-) + \sum_{i \neq j,\nu} \lambda_\nu (\sigma_{i\nu}^- \sigma_{j\nu}^+ + \sigma_{i\nu}^+ \sigma_{j\nu}^-), \quad (6c)$$

where

$$\lambda_i = -\frac{g^2}{2(\Delta_i - \omega_{\text{at}})}, \quad (7a)$$

$$\lambda_\nu = -\frac{g^2}{2(\Delta_\nu - \omega_{\text{at}})} \quad (7b)$$

are the effective spin–spin couplings along the rows (columns) and

$$\delta \omega_{\text{at},i\nu} = \lambda_i (2a_i^\dagger a_i + a_i^\dagger b_\nu + b_\nu^\dagger a_i) + \lambda_\nu (2b_\nu^\dagger b_\nu + a_i^\dagger b_\nu + b_\nu^\dagger a_i). \quad (8)$$

2.3. Validity of the approximations and frustrated versus non-frustrated regime

Dispersively eliminating photonic or phononic fields leading to an effective spin physics is a known technique often used in the design of various quantum optical simulators. It can lead to interesting frustrated spin Hamiltonians, e.g. in the context of trapped ions [39, 40, 54].

In order to simplify the parameter space, in what follows we choose all the couplings to be the same along rows (columns): $\lambda_a \equiv \lambda_i$, $\forall i$ ($\lambda_b \equiv \lambda_\nu$, $\forall \nu$). Schematically, the parameter regime of the spin Hamiltonian (5) is summarized in figure 1(d).

First we note, that the parameters $\omega_{\text{at}}/2$, λ and $\delta \omega_{\text{at}}$ of the Hamiltonian (5) given by (3a), (7) and (8) can take both positive or negative sign. In particular the sign of λ determines the kind of physical situation provided by the interaction Hamiltonian (6c): *non-frustrated* if both couplings are negative, $\lambda_{a(b)} < 0$ and *frustrated* otherwise. This is apparent from the form of the interaction which tends to align each pair of spins antiparallel whenever the corresponding coupling is positive. This then leads to frustration as the antiparallel alignment cannot be satisfied simultaneously for all the spins. Note that while we consider square lattice for concreteness, the presence of frustration in cavity arrays stems from all-to-all interaction between spins belonging to the same cavity mode and, hence, is independent of the lattice geometry.

Next, we discuss the parameter regimes of the Hamiltonian (5). We recall that the only requirement used in the derivation of (5) from the parent TC Hamiltonian (2) is the condition (4), $g \ll |\omega_{\text{at}} - \Delta_{a(b)}|$.

(i) *Weakly interacting regime*. We refer to the weakly interacting regime as the regime where (we drop the a , b indices for simplicity)

$$|\lambda_{a(b)}| \ll |\omega_{\text{at}}|. \quad (9)$$

Here, we have neglected the $\delta\omega_{\text{at}}$ term contributing to the atomic transition frequency since $\delta\omega_{\text{at}} \propto \lambda^4$. One should verify that reaching the weakly interacting regime is compatible with the conditions (1) and (4) used in the derivation of the Hamiltonians (2) and (5). It is easy to show that it is indeed the case: substituting (7) for λ in (9), we get $|g^2/\omega_{\text{at}}| \ll |\Delta - \omega_{\text{at}}|$. This implies, together with (4), that $|g| \lesssim |\omega_{\text{at}}|$. Finally, substituting for g from (3b), we get $|g_0| \lesssim |\Omega|$. This is enforced by the stronger condition (1), which completes our consistency check.

(ii) *Strongly interacting regime.* We refer to the strongly interacting regime as the regime where $|\lambda_{a(b)}| \gtrsim |\omega_{\text{at}}/2 + \langle\delta\omega_{\text{at}}\rangle|$. Here, the cavity fields dependence of the $\delta\omega_{\text{at}}$ term plays an essential role. We leave this interesting possibility for section 5 and focus first on the scenario where the dynamics of the cavity fields decouples from the spins leading to a pure spin Hamiltonian.

2.4. Comment on experimental realizations

While cavity QED has become a well established experimental research direction, a brief discussion of whether the ground state physics studied in this paper can be accessed in a realistic experiment is in order. We note that since the excited state $|e\rangle$ has been eliminated, the atoms are assumed to be trapped at the positions of the lattice sites and the levels $|0\rangle$, $|1\rangle$ correspond to the long-lived hyperfine states, the main decoherence mechanism is due to the decay κ of the cavity modes (we consider the same decay rate for all modes). In order to estimate whether one can reach the ground state of the spin Hamiltonian (5), we consider an adiabatic preparation scheme, i.e. a situation where the parameters of the Hamiltonian are tuned sufficiently slowly so that the state of the system at a given time is also its ground state [55]. Specifically, the rate of change of the Hamiltonian parameters r should be much smaller than the energy gap ΔE between the ground and the first excited state in order to avoid level mixing, $r \ll \Delta E$. Provided ω_{at} is the largest energy scale in (5), the gap corresponds to the energy cost of exciting a single spin, i.e. $\Delta E \approx \omega_{\text{at}}$. At the same time, r should be much faster than the cavity decay in order to be able to reach the desired ground state without being affected by the decay, which yields the following condition for the timescales

$$|\omega_{\text{at}}| \gg r \gg \kappa \Rightarrow |\omega_{\text{at}}| \gg \kappa. \quad (10)$$

Using (3a) and the fact that $\Delta_e \gg \Omega \gg g_0$ (see equation (1) and the discussion above it) we arrive at $|\omega_{\text{at}}| \gg g_0$ provided $\Omega/g_0 \gg \Delta_e/\Omega$. Therefore one can see, that the condition (10) is automatically fulfilled in the strong coupling regime, where $g_0 \gtrsim \kappa$. This regime has been realized in a number of platforms, such as optical microcavities [56], fibre-based cavity on atomic chip [57] or open-access on-chip microcavities [52] all combined with ^{87}Rb atoms with $(g_0, \kappa) \approx 2\pi \times (25, 2.5)$ MHz, $2\pi \times (250, 50)$ MHz and $2\pi \times (1, 6.5)$ GHz for [56, 57] and [52] respectively.

Other elements required to realize the proposed setup have been also achieved experimentally, such as a creation of optical lattices with unit filling using optical tweezer arrays [58, 59] or in principal arbitrary geometries of silica-engraved waveguide arrays [30–32]. While those elements, together with the condition (10), are within reach of current technology, their combination on a single device remains a challenge. Fortunately, there are active experimental efforts to achieve this goal, for example to combine the waveguide arrays with atomic microtraps [51] or atoms with photonic-crystal nanocavities [60].

3. 1D: exact solution of the spin model

It is illustrative to clarify on a simple example some of the basic properties of the Hamiltonian (5). Specifically, we are interested in the nature of phase transitions featured by (5) and the scalings of critical couplings. To this end we consider a one-dimensional limit of (5) by taking a single cavity mode a . The Hamiltonian simplifies to

$$H_{\text{spin}}^{\text{1D}} = \Delta a^\dagger a + [\omega_{\text{at}} + 4\lambda a^\dagger a]J^z + 2\lambda J^+ J^-. \quad (11)$$

Here, J are the total angular momentum operators

$$J^l = \frac{1}{2} \sum_{i=1}^N \sigma_i^l, \quad l = x, y, z, \quad (12a)$$

$$J^\pm = \sum_{i=1}^N \sigma_i^\pm. \quad (12b)$$

We note that in the absence of the cavity fields, (11) is the well-known Lipkin–Meshkov–Glick model [61], which has been recently studied also in the context of cavity QED [62]. The advantage of the model (11) is that it is exactly solvable providing us with useful analytical insights. Using the usual angular momentum algebra

⁴ One should verify the self-consistency of the condition (9) when performing the simulation of the parent TC model, i.e. to check, whether the resulting cavity occupation is such that $|\langle\delta\omega_{\text{at}}\rangle| \ll |\omega_{\text{at}}|$.

Table 1. Summary of phase transitions as the coupling $g(\lambda)$ is varied in the 1D effective spin model (11) based on the analysis of (14). + (−) stand for positive (negative) values respectively. The ‘($n = \infty$)’ description in the second and fifth line indicates that in these cases, the ground state corresponds to the infinite photon number independently of the value of λ , see (15) and text for details.

ω_{at}	Ground state configuration (for $\lambda = 0$)	λ	$\Delta - \omega_{\text{at}}$	Δ	Spin transition
+	$ 0 \dots 0\rangle$	+	−	+	no
		+	−	−	no ($n = \infty$)
		−	+	+	yes
−	$ 1 \dots 1\rangle$	−	+	−	yes
		−	+	+	no ($n = \infty$)
		+	−	−	no

$$J^z|J, m\rangle = m|J, m\rangle, \quad (13a)$$

$$J^{\pm}|J, m\rangle = \sqrt{J(J+1) - m(m \pm 1)}|J, m \pm 1\rangle, \quad (13b)$$

where J is the half-integer total angular momentum ($J = N/2$ for N spins) and $m = -J, -J+1, \dots, J$, it follows that $|J, m, n\rangle$, where n is the photon number, are the eigenstates of the Hamiltonian (11). The eigenenergies are

$$\begin{aligned} E_{J,m,n} &= \Delta n + [\omega_{\text{at}} + 4\lambda n]m + 2\lambda[J(J+1) - m(m-1)] \\ &= [\Delta + 4\lambda n]n + 2\lambda[J(J+1) - m(m-1)] + \omega_{\text{at}}m, \end{aligned} \quad (14)$$

where in the second line we have regrouped the terms in order to emphasise the dependence on the photon number n .

The implications of the first bracket in the second line of (14) are the following. For

$$E_n \equiv \Delta + 4\lambda m > 0 \quad (15)$$

the ground state photon number is 0. On the other hand, for $E_n < 0$ the ground state photon number is $n = \infty$, which invalidates the approximate description in terms of the effective Hamiltonian (11). At this point it is important to note that since both $\Delta - \omega_{\text{at}}$ in the denominator of λ and m can take positive or negative values, there is always a combination of m and $\Delta - \omega_{\text{at}}$ where the transition $n = 0 \leftrightarrow n = \infty$ occurs as λ is varied. The situation is summarized in table 1. The main message contained in the table 1 is that it is *not* possible to simulate the frustrated spin system using (2) in one-dimension (see also [63]). In section 5 we will show, how this limitation can be circumvented in two-dimensions by exploiting the properties of the $\delta\omega_{\text{at}}$ term (8).

In what follows we shall investigate this transition and its relation to the parent TC Hamiltonian (2) further. The $n = 0 \leftrightarrow n = \infty$ transition occurs when E_n changes sign. From (7) and (15) we get the expression for a critical coupling g_c

$$g_c = \sqrt{\frac{\Delta(\Delta - \omega_{\text{at}})}{2m}}. \quad (16)$$

Lets first consider $\omega_{\text{at}} > 0$. In the non-frustrated case ($\lambda < 0, \Delta > \omega_{\text{at}}$), the minimal possible value of g_c corresponds to $m = N/2$ (i.e. all spins excited). On the other hand, for $\lambda > 0$ and positive ω_{at} assumed here, we can have either $\Delta > 0$ or $\Delta < 0$. For $\Delta < 0$, we can see immediately from (15) that E_n can be made *always* negative by a suitable choice of m . Specifically, considering the spin ground state $m = -N/2$, the global ground state would correspond to $n = \infty$ invalidating the description in terms of (11). On the other hand, for $\Delta > 0$ the system undergoes the $n = 0 \leftrightarrow n = \infty$ transition as λ is increased. However, it occurs for $m = -N/2$, i.e. before any spin transition could possibly take place. One could now proceed analogously for $\omega_{\text{at}} < 0$ ⁵.

In summary, the critical coupling at which the $n = 0 \leftrightarrow n = \infty$ transition occurs is given by

$$g_c^{\text{ph}} = \frac{1}{\sqrt{N}} \sqrt{\Delta(\Delta - \omega_{\text{at}})}, \quad (17)$$

where we have emphasised by the label ‘ph’, that the transition is in the photon number.

In one-dimension, the only non-trivial situation is thus the non-frustrated case, $\lambda < 0$, where $n = 0$. Here, a series of transitions between phases with $N_{\text{exc}}(m)$ and $N_{\text{exc}}(m+1) = N_{\text{exc}}(m) + 1$ excited spins takes place as $|\lambda|$ is increased (here $N_{\text{exc}}(m) = (2m + N)/2$). The corresponding coupling strengths at which these transitions occur are obtained from (14) by solving for $E_{J,m,0} = E_{J,m+1,0}$.

For instance, considering $\omega_{\text{at}} > 0$ and $\Delta > \omega_{\text{at}}$, third line in table 1, the first spin transition from $m = -N/2$ to $m = -N/2 + 1$ occurs at

⁵ We note that (11) does not inherit the simple \mathbb{Z}_2 symmetry of the parent TC model, namely the symmetry under simultaneous exchange $\sigma^z \rightarrow -\sigma^z, \sigma^+ a \rightarrow a^\dagger \sigma^-$ and $\omega_{\text{at}} \rightarrow -\omega_{\text{at}}$, due to the nonlinear nature of the transformation yielding the effective spin model, see appendix A.

$$g_c = \frac{1}{\sqrt{N}} \sqrt{\omega_{\text{at}}(\Delta - \omega_{\text{at}})}. \quad (18)$$

One can also read off from the expression (18) the scaling properties of the critical point of the spin transition with the system size, $g_c \propto 1/\sqrt{N}$ and correspondingly for the critical coupling $\lambda, |\lambda_c| \propto 1/N$.

4. 2D: analytical study and QMC simulations

After having analysed the situation in 1D, we now turn our attention to 2D. It is well known that the Dicke model features second order superradiant phase transition as the coupling strength is varied [33, 64, 65]. We will analyse the scaling properties at this superradiant phase transition and evaluate the two-point spin correlation functions of the cavity array. In order to do so, we employ large scale QMC simulations using the worm algorithm [66, 67]. In the following we compare the QMC results with the MF solutions. We emphasise that in the considered square lattice geometry the spins are *not* all-to-all connected (they are connected only if they belong to the same row/column), i.e. it is not apriori obvious whether the MF solutions provide an accurate quantitative description.

In order to simplify the discussion, in this section we consider equal couplings along all rows and columns, $\lambda \equiv \lambda_a = \lambda_b$ (i.e. $\Delta \equiv \Delta_i = \Delta_\nu, \forall i, \nu$). Motivated by the findings in the one-dimensional case, we focus only on the non-frustrated case with $\omega_{\text{at}} > 0$ and $\Delta > \omega_{\text{at}}$. We will address the frustrated case in section 5.

MF solutions. In the thermodynamic limit, one can find MF solutions of the TC model (2) which we describe in detail in appendix B and which we use for the sake of comparison with the QMC data. In particular, for an array of size $N = L_x \times L_y$ one can find expressions for the critical strength g_c^{MF} of the coupling at which the superradiant transition occurs and the number of spin excitations N_{exc} in the superradiant phase, which read

$$g_c^{\text{MF}} = \sqrt{\Delta \omega_{\text{at}} \left(\frac{L_x + L_y}{4L_x L_y} \right)} \quad (19)$$

and

$$N_{\text{exc}}^{\text{MF}} = \frac{N}{2} \left(1 - \left(\frac{g_c^{\text{MF}}}{g} \right)^2 \right) \quad (20)$$

respectively. In the specific case of a square array $L \equiv L_x = L_y$ and in the limit $\Delta \rightarrow \infty$, where the descriptions in terms of (2) and (5) should coincide, we get with the help of (7)⁶

$$\lambda_c^{\text{MF}, \infty} \equiv -\frac{\omega_{\text{at}}}{4L} \quad (21)$$

and

$$N_{\text{exc}}^{\text{MF}, \infty} \equiv \frac{N}{2} \left(1 + \frac{1}{4L} \frac{\omega_{\text{at}}}{\lambda} \right). \quad (22)$$

The spin model (5) is an effective description of the parent TC model (2) in the limit of large detuning (4). Therefore, the excitations of the TC model in the superradiant phase result in spin excitations in the effective spin model. Here, QMC provides an efficient numerical tool to study this limit behaviour of the TC model and how well it is described by the effective spin model. The results of the simulations are presented in figure 2. Here we show the critical couplings of the superradiant phase transition g_c determined using QMC (using the total number of photonic and spin excitations as order parameter, where the transition separates the normal and superradiant phases characterised by zero (non-zero) value of the order parameter; square and circle data points) and the MF prediction (19), solid and dashed lines. The red (blue) data correspond to two different system sizes $N = 18 \times 18$ ($N = 28 \times 28$) respectively and the horizontal black lines are the values of the critical couplings λ_c obtained from the QMC simulation of the effective spin model (5). As expected, we find that the values of the critical couplings approach asymptotically in the limit $\Delta \gg \omega_{\text{at}}$ where the two models (2) and (5) coincide. In the insets we show the finite size scaling of the critical couplings for the TC (left inset) and effective spin (right inset) models. As in the main plot, the squares represent the QMC data and the solid lines are the MF predictions (19) and (21). The slight departure of the scaling for the spin model for small system sizes is indeed a finite size effect on which we will comment momentarily. We also note, that the couplings for the present 2D model scale in the same way as the 1D predictions (18), i.e. in the linear extent of the system, $g_c \propto 1/\sqrt{L}$. This is due to the fact that the scaling is determined by the number of *cavity modes* to which the atoms couple rather than by the system size N (see also appendix B).

⁶ We note that for the square array, $g_c^{\text{MF}} \propto 1/\sqrt{L}$ and $|\alpha_s|^2 \propto (g - g_c^{\text{MF}})$ in the vicinity of the critical point, see (B5), i.e. we recover the same scaling behaviour as given by the single-mode Dicke model undergoing the superradiant phase transition [65, 76, 77].

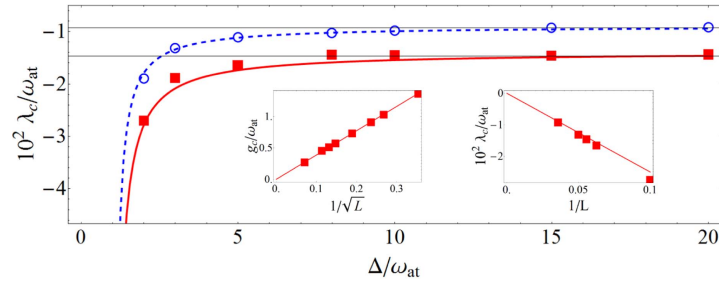


Figure 2. Reaching the effective spin model as the limiting case of the TC Hamiltonian. The main plot shows critical coupling λ_c of the superradiant phase transition as a function of the photon detuning. The squares and circles are the data obtained from the QMC simulation of the TC model (2). The solid lines are the MF predictions (19). The red solid line and squares (blue dashed line and circles) correspond to system sizes $N = L \times L = 18 \times 18$ ($N = 28 \times 28$) respectively. The solid black lines are the critical coupling values obtained from the QMC simulation of the spin model (5) for a given system size. *Left inset:* finite size scaling of the critical coupling of the spin model. We note that the coupling goes to zero in the thermodynamics limit as expected, see equation (19). We have used $\Delta/\omega_{\text{at}} = 30$ in the insets.

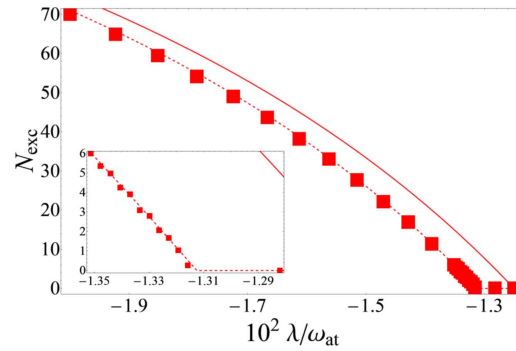


Figure 3. Number of spin excitations of the spin model (5) on $N = 20 \times 20$ array versus the interaction strength λ . The squares represent the QMC data, the solid line is the MF prediction (22). The dashed line is the MF prediction corrected for the finite size offset (see text for details). The inset shows the magnification of the region in the vicinity of the critical coupling.

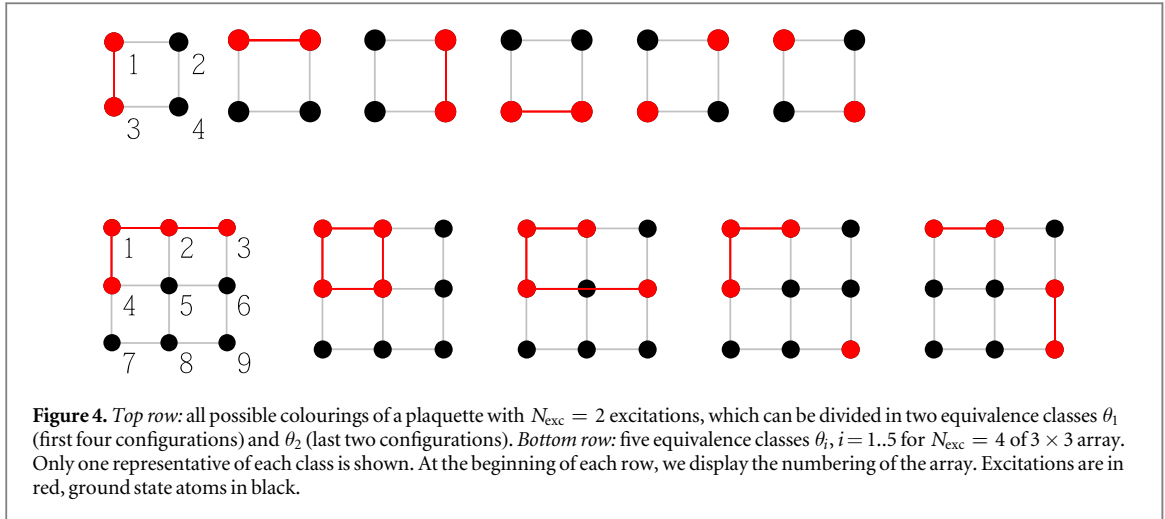
After we have verified that the critical couplings of the TC model coincide with those of the spin model, we now study the number of excitations of the spin model as the coupling strength is varied. This is shown in figure 3. The solid line corresponds to the MF prediction (22). The squares correspond to the QMC simulation of the spin model (5) on a $N = 20 \times 20$ array, where we have neglected λ_a, λ_b in (6a) as $|\lambda| \ll \omega_{\text{at}}$ in the studied regime. The discrepancy between the MF prediction and the QMC simulation is precisely the consequence of neglecting λ_a, λ_b in (6a) and results in an offset $-1/(4L^2)$ in the values of λ —the dashed line corresponds to the MF solution corrected for this offset⁷.

So far, we concentrated only on one-point observables in our QMC simulations and found a good agreement with the MF predictions. In order to go beyond the MF picture we next consider the correlation functions. Before presenting the results and in order to get a deeper insight in the structure of the spin Hamiltonians emergent in cavity arrays, in the following section we study the properties of the ground states from the group and graph theory perspective.

4.1. Ground state structure

Symmetry considerations. We start our analysis in this section by noting that the total number of spin excitations, $\hat{N}_{\text{exc}} = \sum_{i,\nu} \frac{1}{2}(\sigma_{i\nu}^z + 1)$, is the constant of motion of the Hamiltonian (5). This significantly simplifies the problem in that in order to find the ground states of (5), one only needs to solve for the eigenstates of the interaction Hamiltonian (6c)

⁷ In the spin model, the transition point is obtained from $E^{0\text{exc}} = E^{1\text{exc}}$, where $E^{0\text{exc}} = -\frac{\omega_{\text{at}}}{2}N$ is the ground state energy with no spin excitation and $E^{1\text{exc}} = \frac{\omega_{\text{at}}}{2}(-N+2) + 4\lambda(L-1)$ the energy with a single excitation (here we have used (40)). Solving for λ we find $\lambda_c = -\frac{\omega_{\text{at}}}{4L}$ which coincides with the MF result (21). Neglecting the λ terms in ω'_{at} (46) amounts to replacing ω'_{at} by ω_{at} in $E^{0\text{exc}} = E^{1\text{exc}}$ above, yielding the solution $\lambda_c = -\frac{\omega_{\text{at}}}{4(L-1)} \approx -\frac{\omega_{\text{at}}}{4L} - \frac{\omega_{\text{at}}}{4L^2}$, where the last term is the offset used in figure 3.



$$H_{\text{spin,int}}|\psi_{\text{GS}}\rangle = E_{\text{GS}}|\psi_{\text{GS}}\rangle \quad (23)$$

in the given excitation number sector N_{exc} .

The problem can be further simplified by exploiting the real space symmetries of the Hamiltonian (5), similarly to the analysis carried out e.g. for the antiferromagnetic Heisenberg chain [68]. Considering the most symmetric situation, i.e. a square array with equal couplings ($L_x = L_y$, $\lambda_a = \lambda_b$), the discrete symmetry group of the Hamiltonian (5) is $G_{L_x \times L_y} = \{\mathfrak{R}, \mathfrak{C}\} \cup D_4$, where \mathfrak{R} , \mathfrak{C} and D_4 stand for permutation of rows, permutation of columns and the dihedral group of the square array (i.e. successive rotations $r_{\pi/2}$, r_{π} , $r_{3\pi/2}$ by $\pi/2$ and reflections about the horizontal (h), vertical (v) and the two diagonal (p , n) axes of the array) respectively. In order to get use of the symmetries, one has to find the irreducible representations (irreps) of G . While a systematic approach exists for finding irreps of the full symmetric group $S_N = L_x L_y$ [69], the subdued representations of the subgroup $G \subset S_N$ are in general reducible [70, chapter 3]. Motivated by exact diagonalization results, instead of finding the irreps of G , we focus on the graph-theoretical properties of the ground states in what follows.

Let us start with the following observation based on the exact diagonalization results of (6c) in the non-frustrated case $\lambda < 0$ in the simplest non-trivial example, a plaquette (i.e. 2×2 array) with $N_{\text{exc}} = 2$ excitations. The vertices of the plaquette are labeled 1–4, see figure 4. The ground state can be written as

$$|\psi_{\text{GS}}\rangle = \frac{1}{\sqrt{2}}(|\theta_1\rangle + |\theta_2\rangle), \quad (24)$$

where

$$|\theta_1\rangle = \frac{1}{\sqrt{4}}(|1100\rangle + |1010\rangle + |0101\rangle + |0011\rangle), \quad (25)$$

$$|\theta_2\rangle = \frac{1}{\sqrt{2}}(|1001\rangle + |0110\rangle), \quad (26)$$

which we symbolically write as

$$|\theta_i\rangle = \frac{1}{\sqrt{|\theta_i|}} \sum_{j \in \theta_i} |s_j\rangle, \quad (27)$$

where $|s_j\rangle$ is a specific spin configuration and $|\theta_i|$ the number of such configurations belonging to a given set θ_i . This seemingly artificial decomposition of the ground state into $|\theta_1\rangle$ and $|\theta_2\rangle$ is in fact directly related to the colouring of a graph as we now discuss.

Let us start by introducing the notions necessary for our considerations which we then demonstrate on specific examples of the ground state construction. To this end we follow closely the treatment presented in [71].

- Lets consider a set S and a group G acting on S with ranks $|S|$ and $|G|$ respectively.
- For G a discrete group, each element $g \in G$ can be written as a product of j -cycles x_j , $g \rightarrow (x_1^{b_1} x_2^{b_2} \dots x_{|S|}^{b_{|S|}})_g$, where b_j counts how many j -cycles appear in the decomposition of g . The product $(x_1^{b_1} x_2^{b_2} \dots x_{|S|}^{b_{|S|}})_g$ is thus a monomial representing the cycle structure of the element g
- Lets consider m colours c_1, \dots, c_m such that a specific colour c_j is assigned to each element of S

Definition 1. A *colouring* C is a specific configuration of colours on S .

For example, considering two colours (black and red), $\bullet, \color{red}\bullet$ is a possible colouring of a plaquette.

Definition 2. An *orbit* of a colouring C is a set of all colourings produced by the action of the group G on C , $\text{orb}_G(C) = \{g(C), g \in G\}$

An orbit is thus an *equivalence class* of all colourings belonging to the orbit.

Definition 3. A *stabilizer* of a colouring C is a set of all group elements g which leave C invariant, $\text{stab}_G(C) = \{g \in G, g(C) = C\}$

Definition 4. A *generating function* (or *pattern inventory* or *cycle index*) is a polynomial given by the sum of all monomials of elements of G acting on S

$$P_G(x_1, \dots, x_{|S|}) = \frac{1}{|G|} \sum_{g \in G} (x_1^{b_1} x_2^{b_2} \dots x_{|S|}^{b_{|S|}})_g. \quad (28)$$

With the definitions above we now introduce two theorems:

Theorem 1. *Pólya's enumeration theorem* [72]. Let $\mathcal{C} = \{C\}$ be a set of all colourings of S using colours c_1, \dots, c_m . Let G induce an equivalence relation on \mathcal{C} Then

$$P_G\left(\sum_{i=1}^m c_i, \sum_{i=1}^m c_i^2, \dots, \sum_{i=1}^m c_i^{|S|}\right) \quad (29)$$

is the generating function for the number of non-equivalent colourings of S in \mathcal{C} .

Theorem 2. *Orbit-stabilizer theorem* [73, 74, chapter 7].

$$|\text{orb}_G(C)| = \frac{|G|}{|\text{stab}_G(C)|}. \quad (30)$$

Equipped with the necessary notions, we return back to the example of the ground state (24)⁸. In order to find the structure of the ground state corresponding to a given excitation number sector N_{exc} , we need to enumerate the number of the sets θ and how many elements belong to each of the set. Here, we are concerned only with two colours, say black and red, which correspond to spins in ground and excited state respectively. In other words, θ is precisely an orbit and $|\theta|$ is thus given by the orbit-stabilizer theorem. We now demonstrate the use of the above theorems on our example of (24). The generating functional (28) of the $G_{2 \times 2} = \{\mathfrak{R}, \mathfrak{C}\} \cup D_4 = D_4$ group of the plaquette reads (see footnote 7)

$$\begin{aligned} P_{G_{2 \times 2}} &= \frac{1}{8}(x_1^4 + 2x_1^2 x_2 + 3x_2^2 + 2x_4) \\ &= b^4 + b^3 r + 2b^2 r^2 + b r^3 + r^4. \end{aligned} \quad (31)$$

In the second line, we have used the Pólya's theorem, where we have substituted the black (b) and red (r) colours, $x_j = b^j + r^j$ for $j = 1, 2, 4$. In our example of two excitations, i.e. the term with r^2 in (31), the numerical prefactor 2 means there are two equivalence classes θ_1, θ_2 of the colourings. These can be found explicitly and read

$$\begin{aligned} \theta_1 &\equiv \text{orb}_{G_{2 \times 2}}(\color{red}\bullet\bullet) = \{\color{red}\bullet\bullet, \color{red}\bullet\bullet, \color{red}\bullet\bullet, \color{red}\bullet\bullet\} \\ \text{stab}_{G_{2 \times 2}}(\color{red}\bullet\bullet) &= \{e, h\}, \\ \theta_2 &\equiv \text{orb}_{G_{2 \times 2}}(\color{red}\bullet\bullet) = \{\color{red}\bullet\bullet, \color{red}\bullet\bullet\} \\ \text{stab}_{G_{2 \times 2}}(\color{red}\bullet\bullet) &= \{e, r_\pi, p, n\}, \end{aligned} \quad (32)$$

where e stands for the identity element of the group G . Finally, one can verify that the above relations obey the orbit-stabilizer theorem (30) so that $|\theta_1| = 4$ and $|\theta_2| = 2$ with the states written explicitly in (26).

The above results can be generalised straightforwardly to larger arrays. In that case the ground state can be written as

$$|\psi_{\text{GS}}\rangle = \sum_i \psi_i |\theta_i\rangle, \quad (33)$$

⁸ The example of colouring of a plaquette is carried out in great detail in [72] and we refer the reader to this reference for further information.

where the orbit states $|\theta_i\rangle$ are orthonormal, $\langle\theta_i|\theta_j\rangle = \delta_{ij}$. To give an explicit example going beyond the plaquette, we consider a 3×3 array and we choose $N_{\text{exc}} = 4$ sector. We find that the total of $\binom{9}{4} = 126$ spin basis states form five equivalence classes depicted in figure 4.

The Hamiltonian in the orbit states basis $\{|\theta_1\rangle, |\theta_2\rangle, |\theta_3\rangle, |\theta_4\rangle, |\theta_5\rangle\}$ reads

$$H_{\text{spin,int}} = \begin{pmatrix} 3 & 0 & 2 & 2 & 2 \\ 0 & 0 & 4 & 0 & 0 \\ 2 & 4 & 2 & 4 & 0 \\ 2 & 0 & 4 & 4 & 4 \\ 2 & 0 & 0 & 4 & 0 \end{pmatrix}. \quad (34)$$

We note that $\langle\theta_2|H_{\text{spin,int}}|\theta_2\rangle = \langle\theta_5|H_{\text{spin,int}}|\theta_5\rangle = 0$. This can be easily understood when inspecting the structure of θ_2 , θ_5 and realizing that the action of the Hamiltonian (6c) is to annihilate an excitation at a given site and create an excitation at another site. It can be seen from figure 4 that such operations necessarily take a state belonging to θ_2 or θ_5 out of its equivalence class. For instance for the example of θ_2 in figure 4, annihilating the excitation at position 5 and creating an excitation at position 6 results in the state θ_3 shown and the corresponding non-zero matrix element $\langle\theta_2|H_{\text{spin,int}}|\theta_3\rangle$ in (34) (in fact an operation displacing *two* excitations at once would be required for the state to remain in θ_2).

The main result of the present discussion is that the set of states (27), which has a clear group-theoretical interpretation in terms of equivalence classes of a coloured graph, constitutes a natural basis for the ground state of the system. While it provides a useful insight into the structure of the ground state, it does not represent a clear computational advantage as we did not provide a prescription for obtaining the Hamiltonian (6c) in the $\{|\theta_i\rangle\}$ basis. Such prescription is likely to be equivalent to finding the irreps of G as discussed at the beginning of this section. We leave this investigation for future work and restrict ourselves only to exact diagonalization in the comparative QMC study of the correlations presented in the following section.

4.2. Correlations

We are now in position to study the correlation functions of the spin model. To this end we consider (connected) two-point correlations of the type $\langle\sigma_{i\nu}^+\sigma_{j\mu}^-\rangle$. Due to long (infinite) range connectivity along the rows and the columns, the system features only two length scales corresponding to spins belonging to the same cavity mode (intra-cavity spins, IC) and to different cavity modes (extra-cavity spins, EC) respectively as there are at most two different cavity modes connecting any two spins of the array. We thus define two types of correlation functions, $\Sigma_{\text{IC}} \equiv \{\langle\sigma_{i\nu}^+\sigma_{i\mu}^-\rangle, \nu \neq \mu\} \cup \{\langle\sigma_{i\nu}^+\sigma_{j\mu}^-\rangle, i \neq j\}$ and $\Sigma_{\text{EC}} \equiv \{\langle\sigma_{i\nu}^+\sigma_{j\mu}^-\rangle, i \neq j, \nu \neq \mu\}$, where we have excluded self-correlations of the type $\langle\sigma^+\sigma^-\rangle = \langle|1\rangle\langle 1|$. This situation is schematically depicted in the inset of figure 5(a). Here, Σ_{IC} corresponds to correlations between the spin in the green box and the spins belonging to the same row and column (red-shaded region). Similarly, Σ_{EC} corresponds to correlations between the spin in the green box and the spins belonging to the blue-shaded region. In figure 5 we plot the ratio $\Sigma_{\text{EC}}/\Sigma_{\text{IC}}$ as a function of the number of spin excitations N_{exc} in an $N = 3 \times 3$ (figure 5(a)) and $N = 5 \times 5$ array (figure 5(b)). For the 3×3 array we find perfect agreement between the exact results obtained by exact diagonalization of the spin Hamiltonian (6c) in each excitation sector and the QMC simulation of that hamiltonian⁹. Moreover we find a good agreement also with the QMC simulation of the TC model (2), which is improving with increasing value of $\Delta/\omega_{\text{at}}$ as it should. Similar agreement between the QMC simulations of the spin and the TC model is observed for the 5×5 array.

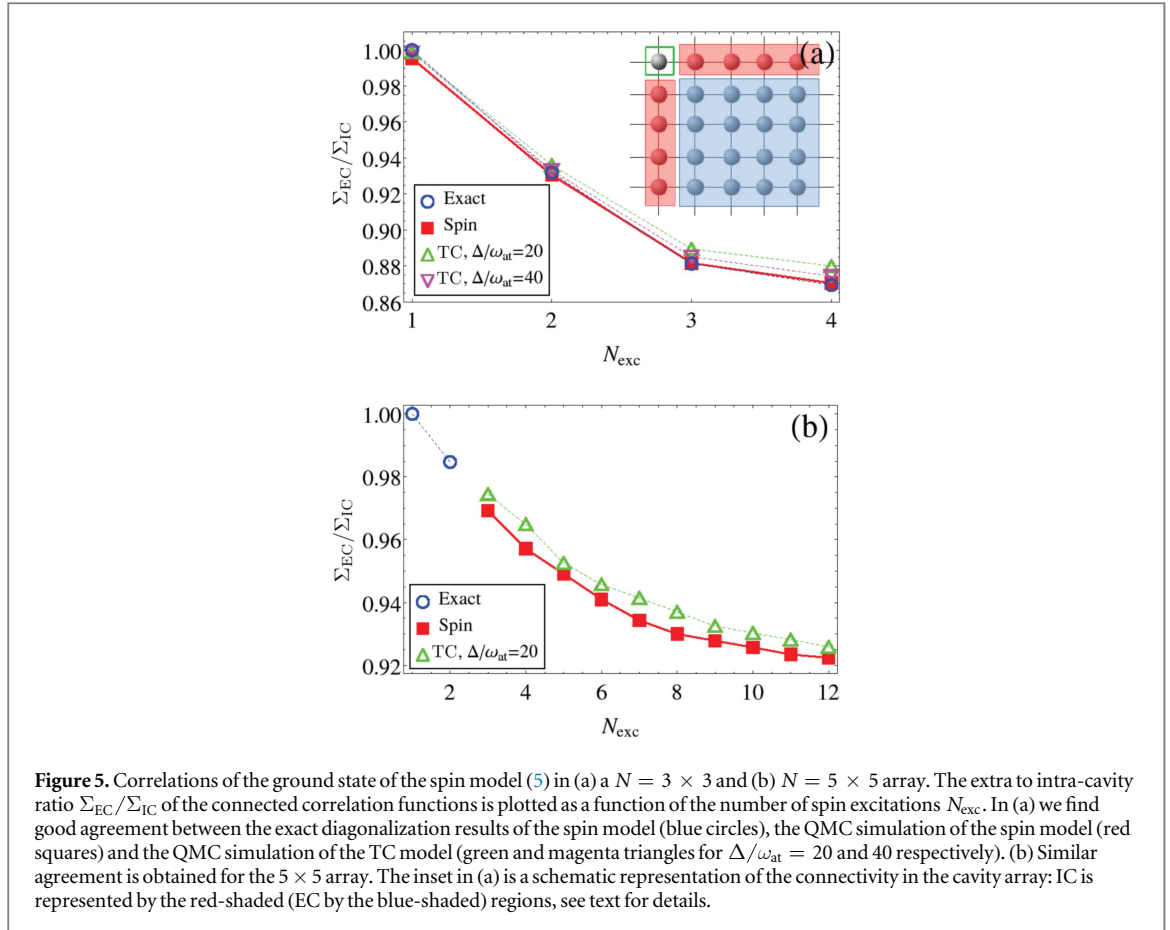
5. Towards simulation of frustrated spin systems in cavity arrays

In section 3 we have shown, that in one-dimension it is not possible to obtain the effective spin Hamiltonian (5) with frustrated interactions $\lambda > 0$. The aim of this section is to show that this limitation can be circumvented in two-dimensions by exploiting the properties of the $\delta\omega$ term (8).

In order to see this, we first perform a back-of-the-envelope estimation. The reason of the breakdown of the effective model in the frustrated case in one-dimension is that as λ is decreased, the term $\lambda a^\dagger a$ in (11) is decreasing in a way that the $n = 0 \leftrightarrow n = \infty$ transition occurs before any spin excitation can appear.

In order to simplify the analytical treatment, from now on we assume all the couplings along rows to be the same, $\lambda_a \equiv \lambda_i$, $\forall i$ and similarly for the columns, $\lambda_b \equiv \lambda_\nu$, $\forall \nu$. Assuming further that the row (column) cavity photon occupation numbers are n_a (n_b), the expectation value of the $\delta\omega$ term (8) becomes

⁹ The QMC simulation is by construction performed in grand-canonical ensemble. The values of $\Sigma_{\text{EC}}/\Sigma_{\text{IC}}$ were obtained by post-selecting on the results with integer number of excitations, $\sum_{i,\nu} \langle n_{i\nu} \rangle = N_{\text{exc}}$.



$$\langle \delta\omega \rangle = 2(\lambda_a n_a + \lambda_b n_b) + \sqrt{n_a n_b} (\lambda_a + \lambda_b) + (\lambda_a + \lambda_b). \quad (35)$$

It is apparent from the above expression that the magnitude of $\langle \delta\omega \rangle$ can be made small when the couplings along rows and columns have opposite signs, $\lambda_a = -\lambda_b$, so that the amplitude of each bracket in (35) becomes significantly smaller than if we take both λ with the same sign. We will thus consider a scenario with frustrated interactions along one direction (we choose the a cavity modes) and non-frustrated one along the other (b modes) and we paramterize the couplings as

$$\lambda_a > 0, \quad \lambda_b < 0, \quad \lambda_b = \eta \lambda_a. \quad (36)$$

In order to show that one can get a non-trivial frustrated–non-frustrated situation without breaking the effective spin description, we will use a self-consistency argument as follows. First we restore the free cavity fields terms we omitted in (5) so that the effective spin Hamiltonian can be written as (see appendix A)

$$H = H_{ph} + H_{spin,int} \quad (37)$$

where

$$H_{ph} = \Delta_a \sum_j a_j^\dagger a_j + \Delta_b \sum_\mu b_\mu^\dagger b_\mu + \sum_{j=1}^{L_x} \sum_{\mu=1}^{L_y} \delta\omega_{at,j\mu} \sigma_{j\mu}^z \quad (38)$$

is now the photonic part (note that we have absorbed the δH term (6b) in H_{ph}) and $H_{spin,int}$ is given by (6c). Exploiting the fact that the σ^z term is diagonal in eigenstate basis in all excitation sectors N_{exc} of the spin Hamiltonian (5), we substitute the spin expectation values $\langle \sigma^z \rangle$ in (38) and subsequently diagonalize the photonic Hamiltonian, which is a straightforward exercise as it is quadratic in the photonic degrees of freedom. We then compare the values of the critical couplings at which a transition $N_{exc} \rightarrow N_{exc} + 1$ occurs with that of $0 \rightarrow \infty$ photon number in analogy to the analysis in section 3. We anticipate that a non-trivial frustrated regime can be always obtained by appropriate tuning of the system parameters and in particular its geometry. This is also the regime which fulfills the self-consistency criterion, namely taking $\langle \delta\omega \rangle = 0$ in the spin model, using the corresponding solutions in the photonic Hamiltonian (38) and finding that its solutions again yield $\langle \delta\omega \rangle = 0$.

5.1. Diagonalization of the spin Hamiltonian

In analogy to section 4 we seek to diagonalize the interaction part of the spin Hamiltonian (6c)

$$H = \lambda_a \sum_{j=1}^{L_x} \sum_{\mu \neq \nu=1}^{L_y} \sigma_{j\mu}^+ \sigma_{j\nu}^- + \lambda_b \sum_{\alpha=1}^{L_y} \sum_{k \neq l=1}^{L_x} \sigma_{k\alpha}^+ \sigma_{l\alpha}^- + \text{h.c.},$$

where we have now explicitly written the summation limits.

0-excitation sector. Here the situation is trivial, the unique ground state being simply $|\psi^0\rangle = |00 \dots 0\rangle$, i.e. all spins down and correspondingly $s_{l\mu}^z \equiv \langle \psi^0 | \sigma_{l\mu}^z | \psi^0 \rangle = -1$, $\forall l, \mu$

1-excitation sector. In the basis $\{|100 \dots 0\rangle, |010 \dots 0\rangle, \dots, |000 \dots 1\rangle\}$ of single particle states, the interaction Hamiltonian (6c) takes a simple form

$$H_{\text{exc}} = 2\lambda_a M_a \otimes \mathbb{1}_b + 2\lambda_b \mathbb{1}_a \otimes M_b, \quad (39)$$

where the a (b) matrices have dimensions $L_x \times L_x$ ($L_y \times L_y$) respectively and the prefactor 2 comes from accounting twice for each spin configuration in (6c). M are matrices with 1 everywhere except the diagonal, where it is 0, $M_{ij} = 1 - \delta_{ij}$. The corresponding eigenvalues and multiplicities are

Matrix	Eigenvalue	Multiplicity
M_a	-1	$L_x - 1$
	$L_x - 1$	1
M_b	-1	$L_y - 1$
	$L_y - 1$	1

Since $\lambda_a > 0$ and $\lambda_b < 0$, the minimum energy is

$$E_{\text{min}}^{\text{exc}} = -2\lambda_a + (L_y - 1)2\lambda_b \quad (41)$$

with multiplicity $L_x - 1$. The corresponding eigenvectors are

$$E_a = -1 \rightarrow |v_a^j\rangle = \frac{1}{\sqrt{2}}(|1_1\rangle - |1_j\rangle), \quad j = 2 \dots L_x, \quad (42)$$

$$E_b = L_y - 1 \rightarrow |v_b\rangle = \frac{1}{\sqrt{L_y}} \sum_{j=1}^{L_y} |1_j\rangle, \quad (43)$$

where $|1_j\rangle \equiv |0 \dots 01_j 0 \dots 0\rangle$. The ground state eigenvectors of H_{exc} are then $|\psi_j^0\rangle = |v_a^j\rangle \otimes |v_b\rangle$ and the spin expectation values become

$$\langle \psi_j^0 | \sigma_{l\mu}^z | \psi_j^0 \rangle = \frac{1}{2L_y} - \left(1 - \frac{1}{2L_y}\right) = -1 + \frac{1}{L_y} \quad (44)$$

if $|\psi_j^0\rangle$ contains an excitation at site $l\mu$ or -1 otherwise. We note that $s_{l\mu}^z \rightarrow -1$ in the thermodynamic limit as one would expect.

In summary, we have for the ground state energies

$$E_{\text{GS}}^{\text{exc}} = \frac{\omega'_{\text{at}}}{2}(-N), \quad (45a)$$

$$E_{\text{GS}}^{\text{exc}} = \frac{\omega'_{\text{at}}}{2}(-N + 2) - 2\lambda_a + (L_y - 1)2\lambda_b, \quad (45b)$$

where

$$\omega'_{\text{at}} = \omega_{\text{at}} + 2(\lambda_a + \lambda_b). \quad (46)$$

5.2. Diagonalization of the photonic Hamiltonian

We are now in position to diagonalize the photonic quadratic form (38). In analogy to the previous paragraph, we start our examination in the 0-excitation sector. Here the expectation values of the spin operator is simply $s^z \equiv s_{l\mu}^z = -1$, $\forall l, \mu$, so that the photonic Hamiltonian becomes

$$H_{\text{ph}} = p^\dagger M_{\text{ph}} p, \quad (47)$$

where we have introduced $p = (a_1, \dots, a_{L_y}, b_1, \dots, b_{L_x})^T$. The matrix M_{ph} can be written as

$$M_{\text{ph}} = \begin{pmatrix} W_a & G \\ G^T & W_b \end{pmatrix} \quad (48)$$

with

$$(W_a)_{ij} = \delta_{ij} \left[\Delta_a + 2\lambda_a \sum_{\nu=1}^{L_x} s_{i\nu}^z \right], \quad i, j = 1 \dots L_y, \quad (49)$$

$$(W_b)_{ij} = \delta_{ij} \left[\Delta_b + 2\lambda_b \sum_{l=1}^{L_y} s_{lj}^z \right], \quad i, j = 1 \dots L_x, \quad (50)$$

$$G_{ij} = (\lambda_a + \lambda_b) s_{ij}^z, \quad i = 1 \dots L_y, j = 1 \dots L_x. \quad (51)$$

M_{ph} has the following eigenvalues and multiplicities

Eigenvalue	Multiplicity
$E_a^{\text{ph}} \equiv \Delta_a + 2\lambda_a L_x s^z$	$L_y - 1$
$E_b^{\text{ph}} \equiv \Delta_b + 2\lambda_b L_y s^z$	$L_x - 1$
$E_+^{\text{ph}} \equiv \frac{1}{2}(\epsilon + \xi)$	1
$E_-^{\text{ph}} \equiv \frac{1}{2}(\epsilon - \xi)$	1

(52)

where

$$\epsilon = \Delta_a + \Delta_b + 2s^z(\lambda_a L_x + \lambda_b L_y), \quad (53a)$$

$$\xi = \sqrt{(\Delta_b - \Delta_a + 2s^z(\lambda_a L_x - \lambda_b L_y))^2 + 4L_x L_y (s^z)^2 (\lambda_a + \lambda_b)^2}. \quad (53b)$$

5.3. Validity and breakdown of the effective spin model

First we note, that due to (36), Δ_b is not independent and can be expressed as

$$\Delta_b = \frac{\Delta_a - \omega_{\text{at}}}{\eta} + \omega_{\text{at}} \quad (54)$$

(here ω_{at} is the bare atomic frequency, not ω'_{at}). Motivated by the condition (4) needed for the spin model (5) to be valid, we define what we call the *quality factor* of the approximation as

$$Q = \min \left(\frac{|\Delta_a - \omega_{\text{at}}|}{g_c^{\text{spin}}}, \frac{|\Delta_b - \omega_{\text{at}}|}{g_c^{\text{spin}}} \right), \quad (55)$$

where g_c^{spin} is given by the critical value of λ_a , $g_c^{\text{spin}} = \sqrt{-2\lambda_{a,c}(\Delta_a - \omega_{\text{at}})}$, see below.

We start by determining the critical value of λ_a at which a transition from 0- to 1-excitation sector occurs in the spin model. This can be simply obtained from the condition $E_{\text{GS}}^{0\text{exc}} = E_{\text{GS}}^{1\text{exc}}$ and with the help of (45) we get

$$\lambda_{a,c}^{\text{spin}} = -\frac{\omega_{\text{at}}}{2\eta L_y}. \quad (56)$$

Next, the breakdown of the effective model is indicated when *any* of the photonic eigenvalues (52) becomes negative, corresponding to infinitely many photons in the ground state. Substituting $s^z = -1$ in (52), the only two candidates for the minimum eigenvalue are E_a^{ph} and E_-^{ph} (we recall that $\lambda_a > 0$, $\lambda_b < 0$). The value of λ_a where E^{ph} becomes negative is determined as

$$\lambda_{a,c}^{\text{ph}} \equiv \min(\lambda_a : E_a^{\text{ph}}(\lambda_a) = 0, E_-^{\text{ph}}(\lambda_a) = 0), \quad (57)$$

where only the positive branch of λ_a in the solutions of $E_-^{\text{ph}}(\lambda_a) = 0$ is considered.

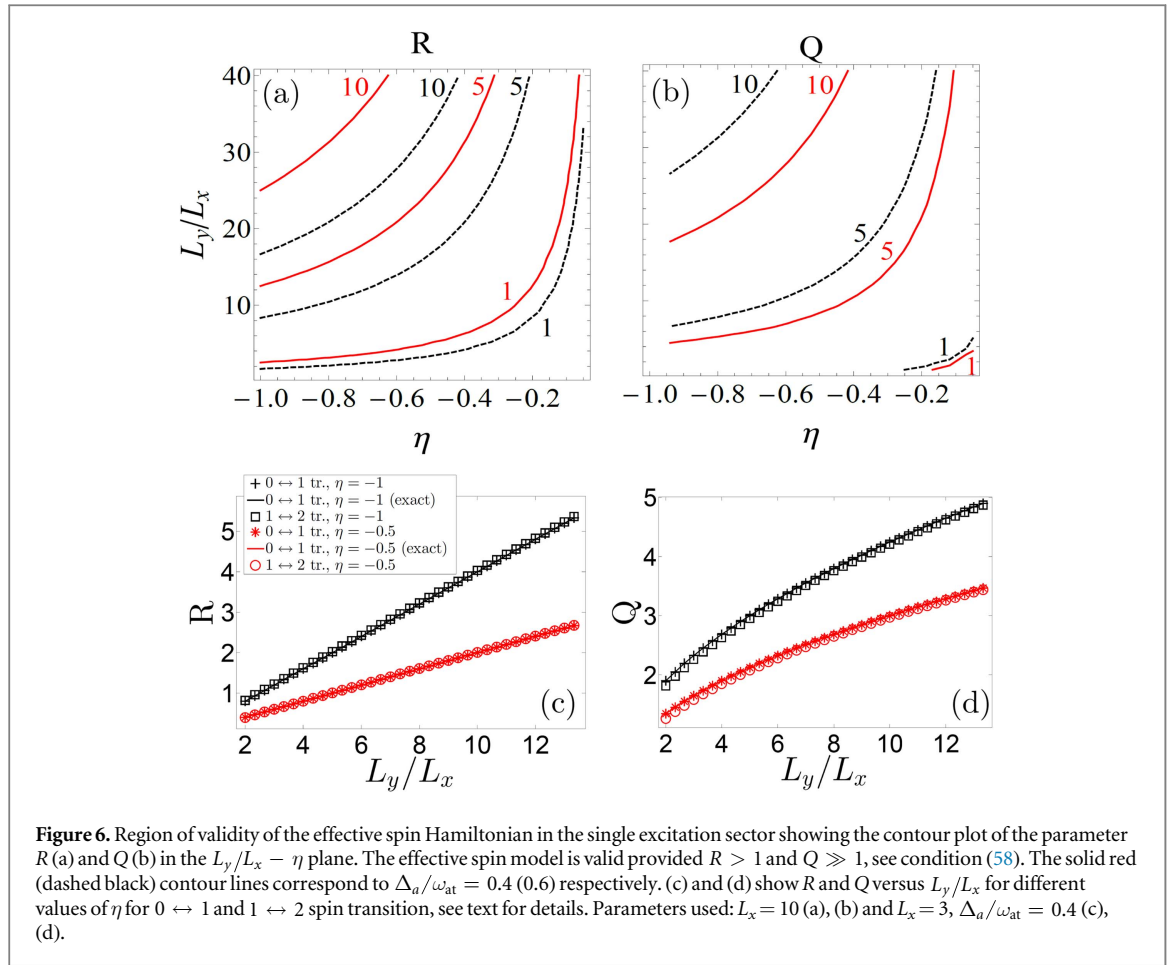
The criterion of having a valid and non-trivial regime in the effective spin Hamiltonian (i.e. finite number of photons and non-zero spin excitations) thus translates into

$$R \equiv \frac{\lambda_{a,c}^{\text{ph}}}{\lambda_{a,c}^{\text{spin}}} > 1 \quad \wedge \quad Q \gg 1. \quad (58)$$

In figure 6 we plot the contours of constant R (a) and Q (b) respectively in the $\eta - L_x/L_y$ plane. It is apparent from the figure that increasing both L_y/L_x and $|\eta|$ leads to a larger critical ratio R , i.e. we can ensure the presence of the non-trivial region by tuning these parameters. Additionally, one can show analytically that

$$\lim_{L_y \rightarrow \infty} R = \infty, \quad (59)$$

$$\lim_{\eta \rightarrow -\infty} R = R_{\text{asymptotic}} \quad (60)$$



when keeping all the other parameters fixed, as expected from the contours in figures 6(a) and (b) (here $R_{\text{asymptotic}}$ is some finite asymptotic value).

So far we have concentrated only on the simple 0 and 1-excitation sectors of the spin Hamiltonian. Clearly, for the interactions to become relevant one is interested in sectors with larger number of excitations.

To this end it is possible to extend the above analysis to the $N_{\text{exc}} \rightarrow N_{\text{exc}} + 1$ spin transitions for $N_{\text{exc}} \geq 1$ and for each of the transitions evaluate the critical ratio R . We note that the fully analytical approach is unfortunately obscured by the fact that for excitation sectors $N_{\text{exc}} > 1$, the spin interaction matrix (6c) does not take the simple structure of (39) and the evaluation of eigenvalues in principle amounts to solving higher order polynomials. Specifically, for a $N_{\text{exc}} \rightarrow N_{\text{exc}} + 1$ spin transition, the critical value of the coupling λ_a can be obtained from the condition $E_{\text{GS}}^{N_{\text{exc}}} = E_{\text{GS}}^{N_{\text{exc}}+1}$, where $E_{\text{GS}}^{N_{\text{exc}}} = \frac{\omega'_{\text{at}}}{2}(-N + 2N_{\text{exc}}) + \delta E^{N_{\text{exc}}}$. Here, $\delta E^{N_{\text{exc}}}$ is obtained from exact diagonalization of (6c). Furthermore, in order to evaluate the critical value of λ_a for the photonic transition (57) (needed for the evaluation of R , (58)), we assume $s_{l\mu}^z = s^z$, $\forall l, \mu$ in (48), where we take $s^z(N_{\text{exc}}) = -1 + \frac{2N_{\text{exc}}}{N}$.

In practice, the restriction of the Hamiltonian to a given N_{exc} sector clearly simplifies the analysis, however the number of basis states still grows rapidly as $\binom{N}{N_{\text{exc}}}$ and an extensive numerical investigation of higher excitation number sectors goes beyond the scope of the present article. For that reason, and in order to unambiguously show that the frustrated regime can be reached in the relevant $N_{\text{exc}} > 1$ sector, we focus on the simplest such situation, namely the $1 \rightarrow 2$ spin transition. In figure 6 we plot R (c) and Q (d) for two distinct values of η ($\eta = -1$ and $\eta = -0.5$) for $0 \leftrightarrow 1$ and $1 \leftrightarrow 2$ spin transition. The solid lines correspond to the analytical result (56) and coincide with the exact diagonalization results for the $0 \leftrightarrow 1$ (black crosses and red stars for $\eta = -1$ and $\eta = -0.5$ respectively)¹⁰. It is apparent from figures 6(c) and (d) that the desired parameter range $R > 1$, $Q \gg 1$ can be achieved also for the $1 \leftrightarrow 2$ spin transition and therefore the frustrated regime can be indeed reached (this is also a confirmation of the intuitive expectation based on the analysis of the $0 \rightarrow 1$ transition alone, namely that the arbitrarily large values of R are a strong indication that higher excitation

¹⁰ The difference in numerical values of R and Q between figures 6(a)–(d) for a given η is a consequence of the fact that they depend not only on the ratio L_y/L_x but also on the value of L_x which is different for (a), (b) [$L_x = 10$] and (c), (d) [$L_x = 3$]. Importantly, the change in the behaviour is not qualitative, but only quantitative.

number sectors can be reached without breaking the validity of the spin Hamiltonian). The smallness of the change of R and Q between the $0 \leftrightarrow 1$ and $1 \leftrightarrow 2$ transitions is a consequence of the fact that the difference between the critical values of λ_a for two adjacent excitation numbers spin transitions ($N_{\text{exc}} \rightarrow N_{\text{exc}} + 1$ and $N_{\text{exc}} + 1 \rightarrow N_{\text{exc}} + 2$) decreases rapidly with the system size (another manifestation of this is the finite size scaling of the superradiant phase transition, see the insets of figure 2, where the critical coupling tends to 0 in the thermodynamic limit.)

To recap, we have shown that the spin model (5) with both frustrated and non-frustrated interactions can emerge as an effective description of the parent TC Hamiltonian (2). This can be achieved when considering an elongated geometry of the square array, $L_y \gg L_x$. On one hand this circumvents the limitations related to realizing effective spin Hamiltonians with frustrated interactions using optical setups governed by TC Hamiltonians [63]. Finally, we note that one can simulate the parent TC model in the regime where it yields the effective spin model using QMC avoiding thus a sign problem of the spin model which opens up an interesting perspective on the QMC simulations of Hamiltonians with sign problem.

6. Conclusions and outlook

In this work we have analysed the ground states of a cavity array where each intersection of cavity modes is occupied by a single atom. We have shown that the system's description in terms of the TC model leads to an effective description—in a suitable parameter regime, where the cavity modes can be dispersively eliminated to first order in the perturbation—in terms of a two-component spin model. In one-dimension, we have provided exact solution of the spin model demonstrating explicitly the need of higher dimensions in order to obtain frustrated spin–spin interactions. Using large-scale QMC simulation of the TC model we have performed a quantitative comparison between the parent TC and the emerging spin model. Specifically, in two-dimensions, we have studied the superradiant phase transition and the properties of two-point correlation functions in the cavity array and we have described the graph-theoretical structure of the ground states of the spin model. In all cases we found a firm agreement between the two models in the regime of validity of the approximations used. Finally, we have outlined the possibility, by exploiting the nonlinearities of the effective spin model, of studying frustrated spin Hamiltonians using two-dimensional cavity arrays.

In conclusion, the theoretical framework and numerical tools established in this work open ways to address the cavity QED physics in a quantitative way beyond the traditional MF or perturbative treatments. The present developments can be exploited in various scenarios, such as the study of the ground state properties in different lattice geometries and dimensions.

Acknowledgments

J M would like to thank Matteo Marcuzzi for useful discussions. The research leading to these results has received funding from the European Research Council under the European Union's Seventh Framework Programme (FP/2007-2013)/ERC Grant Agreement No. 335266 (ESCQUMA) and the EU-FET grants HAIRS 612862 and QuILMI 295293.

Appendix A. Effective spin Hamiltonian in the dispersive regime

We provide the details of the adiabatic elimination of the excited state $|e\rangle$ in our previous publication [53] (note that here we use the basis $\{|e\rangle, |1\rangle, |0\rangle\}$ instead of $\{|e\rangle, |s\rangle, |g\rangle\}$ in [53]). The resulting Hamiltonian reads

$$H = \sum_i \Delta_i a_i^\dagger a_i + \sum_\nu \Delta_\nu b_\nu^\dagger b_\nu + \sum_{i,\nu} \left(\frac{\omega_{\text{at},i\nu}}{2} + \delta\omega_{\text{at},i\nu} \right) \sigma_{i\nu}^z + g(\sigma_{i\nu}^+(a_i + b_\nu) + \text{h.c.}) + F_{i\nu}, \quad (\text{A1})$$

where

$$\begin{aligned} \omega_{\text{at},i\nu} &= -\frac{\Omega^2}{\Delta_e}, \\ \delta\omega_{\text{at},i\nu} &= -\frac{g_0^2(a_i^\dagger + b_\nu^\dagger)(a_i + b_\nu)}{2\Delta_e}, \\ g &= -\frac{g_0\Omega}{\Delta_e}, \\ F_{i\nu} &= -\frac{1}{2\Delta_e}(\Omega^2 + g_0^2(a_i^\dagger + b_\nu^\dagger)(a_i + b_\nu)) \end{aligned} \quad (\text{A2})$$

with $\Delta_x = \omega_x - (\omega_1 + \omega_T)$, $x = i, \nu, e$ and g_0 the coupling strength of the $|1\rangle - |e\rangle$ transition. We take Ω and g_0 to be real and positive throughout the article. Here we have set $\omega_{\text{aux}} = \omega_1 + \omega_T$ in [53] and carried out the adiabatic elimination under the usual condition $|\Delta_e| \gg |\Omega|, |g_0|$.

In this article we focus on the regime, where $|\omega_{\text{at}}| \gg |\langle \delta\omega \rangle|$. This can be in principle always achieved in the limit

$$\Omega \gg g_0. \quad (\text{A3})$$

Neglecting the $\delta\omega$ term (and consequently the F term), the Hamiltonian (A1) simplifies to (2),

$$H_{\text{TC}} = \sum_i \Delta_i a_i^\dagger a_i + \sum_\nu \Delta_\nu b_\nu^\dagger b_\nu + \sum_{i,\nu} \frac{\omega_{\text{at},i\nu}}{2} \sigma_{i\nu}^z + g \sum_{i,\nu} (\sigma_{i\nu}^+(a_i + b_\nu) + (a_i^\dagger + b_\nu^\dagger) \sigma_{i\nu}^-), \quad (\text{A4})$$

which is the usual TC Hamiltonian.

Next we proceed with the derivation of the Hamiltonian (5). From here on we take the bare atomic frequencies to be equal for all atoms, $\omega_{\text{at},i\nu} = \omega_{\text{at}}, \forall i, \nu$. We find the form of the effective spin Hamiltonian after further transformation of the cavity fields. Working in the perturbative dispersive regime

$$\epsilon_{i\nu} = |g/(\omega_{\text{at}} - \Delta_{i(\nu)})| \ll 1, \quad \forall i, \nu, \quad (\text{A5})$$

one can eliminate the cavity fields iteratively by means of unitary transformation to arbitrary order in $\epsilon_{i\nu}$ [75]

$$H_{\text{spin}} = e^S H_{\text{TC}} e^{-S} = H_0^{\text{TC}} + H_{\text{int}}^{\text{TC}} + [S, H_0^{\text{TC}}] + [S, H_{\text{int}}^{\text{TC}}] + \frac{1}{2}[S, [S, H_0^{\text{TC}}]] + \dots, \quad (\text{A6})$$

where $H_0^{\text{TC}}, H_{\text{int}}^{\text{TC}}$ stand for the free and interaction part of the TC Hamiltonian respectively. To first order in $\epsilon_{i\nu}$, the antihermitian matrix S reads

$$S = \frac{g}{\delta_i} (a_i^\dagger \sigma_{i\nu}^- - \sigma_{i\nu}^+ a_i) + \frac{g}{\delta_\nu} (b_\nu^\dagger \sigma_{i\nu}^- - \sigma_{i\nu}^+ b_\nu), \quad (\text{A7})$$

where $\delta_{i(\nu)} = \Delta_{i(\nu)} - \omega_{\text{at}}$. The effective spin Hamiltonian becomes

$$\begin{aligned} H_{\text{spin}} &= H_0^{\text{TC}} + \frac{1}{2}[S, H_{\text{int}}^{\text{TC}}] \\ &= \Delta_i a_i^\dagger a_i + \Delta_\nu b_\nu^\dagger b_\nu + \left(\frac{\omega_{\text{at}}}{2} + \delta\omega_{\text{at},i\nu}^{\text{spin}} \right) \sigma_{i\nu}^z + \lambda_i (\sigma_{i\nu}^- \sigma_{i\mu}^+ + \sigma_{i\mu}^+ \sigma_{i\nu}^-) + \lambda_\nu (\sigma_{i\nu}^- \sigma_{j\nu}^+ + \sigma_{j\nu}^+ \sigma_{i\nu}^-), \end{aligned} \quad (\text{A8})$$

where

$$\begin{aligned} \delta\omega_{\text{at},i\nu}^{\text{spin}} &= \lambda_i (2a_i^\dagger a_i + 1 + a_i^\dagger b_\nu + b_\nu^\dagger a_i) + \lambda_\nu (2b_\nu^\dagger b_\nu + 1 + a_i^\dagger b_\nu + b_\nu^\dagger a_i) \\ \lambda_i &= -\frac{g^2}{2\delta_i} \\ \lambda_\nu &= -\frac{g^2}{2\delta_\nu}. \end{aligned} \quad (\text{A9})$$

Appendix B. MF solution of the TC model

The Hamiltonian of the 2D system considered in section 4 is the following:

$$H_{\text{TC}} = \Delta \left(\sum_i a_i^\dagger a_i + \sum_\nu b_\nu^\dagger b_\nu \right) + \frac{\omega_{\text{at}}}{2} \sum_{i\nu} \sigma_{i\nu}^z + g \sum_{i\nu} (a_i^\dagger \sigma_{i\nu}^- + a_i \sigma_{i\nu}^+) + g \sum_{i\nu} (b_\nu^\dagger \sigma_{i\nu}^- + b_\nu \sigma_{i\nu}^+). \quad (\text{B1})$$

We notice that the number of two-level atoms is $N = L_x \times L_y$ whereas the number of electromagnetic modes is $N_{\text{em}} = L_x + L_y$. This means that for a large 2D array $N \gg N_{\text{em}}$ and we can apply the standard mean field techniques originally introduced in [64, 65]. Since we are interested in the zero temperature limit, we restrict our analysis to this particular case, where the calculation amounts to average the full Hamiltonian over a set of photonic coherent states:

$$|\alpha\rangle_i = e^{-\frac{|\alpha_i|^2}{2}} e^{\alpha_i a_i^\dagger} |0\rangle, \quad |\beta\rangle_\nu = e^{-\frac{|\beta_\nu|^2}{2}} e^{\beta_\nu b_\nu^\dagger} |0\rangle \quad (\text{B2})$$

and to minimize the resulting non-interacting problem with respect to the set of variational complex variables (α_i, β_ν) . By symmetry, the ground state solutions must be of the form $\alpha_i = \beta_\nu = \alpha$ and thus the partial

integration over the photonic degrees of freedom gives the following function of the spins only:

$$H_{\text{TC}}^{\text{MF}} = \Delta(L_x + L_y)|\alpha|^2 + \frac{\omega_{\text{at}}}{2} \sum_{i\nu} \sigma_{i\nu}^z + 2g \left(\alpha \sum_{i\nu} \sigma_{i\nu}^+ + \alpha^* \sum_{i\nu} \sigma_{i\nu}^- \right), \quad (\text{B3})$$

which can be easily diagonalized in each single-atomic subspace, giving as a result for the energy of the ground state:

$$E_{\text{GS}} = \Delta(L_x + L_y)|\alpha|^2 - L_x L_y \sqrt{\left(\frac{\omega_{\text{at}}}{2}\right)^2 + 4g^2|\alpha|^2}. \quad (\text{B4})$$

The minimization of E_{GS} allows us to appreciate two different phases of the system: (i) a phase where the stable solution is $|\alpha|^2 = 0$, which physically corresponds to a zero macroscopic number of atomic excitations in the system (and also to a zero macroscopic number of photons in the cavities, since this number is proportional to $|\alpha|^2$). (ii) A superradiant phase where the stable solution is:

$$|\alpha_s|^2 = \left(\frac{L_x L_y g}{\Delta(L_x + L_y)} \right)^2 - \left(\frac{\omega_{\text{at}}}{4g} \right)^2. \quad (\text{B5})$$

This solution is stable above a critical coupling which is given by:

$$g_c^{\text{MF}} = \sqrt{\frac{(L_x + L_y)\omega_{\text{at}}\Delta}{4L_x L_y}}, \quad (\text{B6})$$

and physically represents the macroscopic number of photons in each cavity mode. In the superradiant phase the atomic ground state reads:

$$|\text{GS}\rangle = \bigotimes_{i,\nu=1}^{L_x L_y} |\text{GS}\rangle_{i\nu}, \quad |\text{GS}\rangle_{i\nu} = \frac{1}{\sqrt{\gamma^2 + 1}} (\gamma|+\rangle_{i\nu} + |-\rangle_{i\nu}), \quad (\text{B7})$$

where $|\pm\rangle_{i\nu}$ are the eigenstates of $\sigma_{i\nu}^z$ with eigenvalues ± 1 and

$$\gamma = \frac{\frac{\omega_{\text{at}}}{2} - \sqrt{\left(\frac{\omega_{\text{at}}}{2}\right)^2 + 4g^2|\alpha_s|^2}}{2g|\alpha_s|}, \quad (\text{B8})$$

This expression can be used to obtain the total number of atomic excitations:

$$\langle \text{GS} | \frac{1}{2} \left(L_x L_y + \sum_{i\nu} \sigma_{i\nu}^z \right) | \text{GS} \rangle = \frac{1}{2} L_x L_y \left(1 - \left(\frac{g_c}{g} \right)^2 \right). \quad (\text{B9})$$

References

- [1] Koch J and Hur K Le 2009 *Phys. Rev. A* **80** 023811
- [2] Schmidt S and Blatter G 2009 *Phys. Rev. Lett.* **103** 086403
- [3] Bhaseen M J, Hohenadler M, Silver A O and Simons B D 2009 *Phys. Rev. Lett.* **102** 135301
- [4] Mering A, Fleischhauer M, Ivanov P A and Singer K 2009 *Phys. Rev. A* **80** 053821
- [5] Silver A O, Hohenadler M, Bhaseen M J and Simons B D 2010 *Phys. Rev. A* **81** 023617
- [6] Nunnenkamp A, Koch J and Girvin S 2011 *New J. Phys.* **13** 095008
- [7] Ciccarello F 2011 *Phys. Rev. A* **83** 043802
- [8] Tan L, Zhang Y-Q and Liu W-M 2011 *Phys. Rev. A* **84** 063816
- [9] Mascarenhas E, Heaney L, Aguiar M and Santos M F 2012 *New J. Phys.* **14** 043033
- [10] Quach J Q 2013 *Phys. Rev. A* **88** 053843
- [11] Zhu G, Schmidt S and Koch J 2013 *New J. Phys.* **15** 115002
- [12] Carusotto I and Ciuti C 2013 *Rev. Mod. Phys.* **85** 299
- [13] Bliokh K, Rodríguez-Fortuño F, Nori F and Zayats A 2015 *Nat. Photon.* **9** 796
- [14] Bliokh K Y, Smirnova D and Nori F 2015 *Science* **348** 1448
- [15] Petersen J, Volz J and Rauschenbeutel A 2014 *Science* **346** 67
- [16] Pichler H, Ramos T, Daley A J and Zoller P 2015 *Phys. Rev. A* **91** 042116
- [17] Ramos T *et al* 2016 *Phys. Rev. A* **93** 062104
- [18] Strack P and Sachdev S 2011 *Phys. Rev. Lett.* **107** 277202
- [19] Gopalakrishnan S, Lev B L and Goldbart P M 2011 *Phys. Rev. Lett.* **107** 277201
- [20] Buchhold M, Strack P, Sachdev S and Diehl S 2013 *Phys. Rev. A* **87** 063622
- [21] Gopalakrishnan S, Lev B L and Goldbart P M 2012 *Phil. Mag.* **92** 353
- [22] Rotondo P, Tesio E and Caracciolo S 2015 *Phys. Rev. B* **91** 014415
- [23] Domokos P and Ritsch H 2002 *Phys. Rev. Lett.* **89** 253003
- [24] Zippilli S, Morigi G and Ritsch H 2004 *Phys. Rev. Lett.* **93** 123002
- [25] Asbóth J K, Domokos P, Ritsch H and Vukics A 2005 *Phys. Rev. A* **72** 053417

- [26] Black A T, Chan H W and Vuletić V 2003 *Phys. Rev. Lett.* **91** 203001
- [27] Baumann K, Guerlin C, Brennecke F and Esslinger T 2010 *Nature* **464** 1301
- [28] Grochol M 2009 *Phys. Rev. B* **79** 205306
- [29] Bermudez A and Plenio M B 2012 *Phys. Rev. Lett.* **109** 010501
- [30] Hartmann M J, Brandao F G S L and Plenio M B 2008 *Laser Photon. Rev.* **2** 527
- [31] Tomadin A and Fazio R 2010 *J. Opt. Soc. Am. B* **27** A130
- [32] Schmidt S and Koch J 2013 *Ann. Phys., Lpz.* **525** 395
- [33] Dicke R H 1954 *Phys. Rev.* **93** 99
- [34] Jaynes E and Cummings F 1963 *Proc. IEEE* **51** 89
- [35] Tavis M and Cummings F W 1968 *Phys. Rev.* **170** 379
- [36] Tavis M and Cummings F W 1969 *Phys. Rev.* **188** 692
- [37] Porras D and Cirac J I 2004 *Phys. Rev. Lett.* **92** 207901
- [38] Deng X-L, Porras D and Cirac J I 2005 *Phys. Rev. A* **72** 063407
- [39] Kim K et al 2009 *Phys. Rev. Lett.* **103** 120502
- [40] Lin G-D, Monroe C and Duan L-M 2011 *Phys. Rev. Lett.* **106** 230402
- [41] Balents L 2010 *Nature* **464** 199
- [42] Savary L and Balents L 2016 *Rep. Prog. Phys.* **80** 016502
- [43] Zhou Y, Kanoda K and Ng T-K 2017 *Rev. Mod. Phys.* **89** 025003
- [44] Schollwöck U 2005 *Rev. Mod. Phys.* **77** 259
- [45] Verstraete F, Murg V and Cirac J 2008 *Adv. Phys.* **57** 143
- [46] Schollwöck U 2011 *Ann. Phys.* **326** 96
- [47] Orús R 2014 *Ann. Phys., NY* **349** 117
- [48] Hohenadler M, Aichhorn M, Schmidt S and Pollet L 2011 *Phys. Rev. A* **84** 041608
- [49] Flottat T, Hébert F, Rousseau V and Batrouni G 2016 *Eur. Phys. J. D* **70** 213
- [50] Marshall G D et al 2009 *Opt. Express* **17** 12546
- [51] Derntl C et al 2014 *Opt. Express* **22** 22111
- [52] Potts C A et al 2016 *Appl. Phys. Lett.* **108** 041103
- [53] Minář J, Söyler Ş G and Lesanovsky I 2016 *New J. Phys.* **18** 053035
- [54] Graß T et al 2016 *Nat. Commun.* **7** 11524
- [55] Messiah A 1999 *Quantum Mechanics* (New York: Dover)
- [56] Sauer J A et al 2004 *Phys. Rev. A* **69** 051804
- [57] Colombe Y et al 2007 *Nature* **450** 272
- [58] Barredo D et al 2016 *Science* **354** 1021
- [59] Endres M, Bernien H, Keesling A, Levine H, Anschuetz E R, Krajenbrink A, Senko C, Vuletić V, Greiner M and Lukin M D 2016 *Science* **354** 1024–7
- [60] Goban A et al 2014 *Nat. Comm.* **5** 3808
- [61] Lipkin H J, Meshkov N and Glick A 1965 *Nucl. Phys.* **62** 188
- [62] Morrison S and Parkins A S 2008 *Phys. Rev. Lett.* **100** 040403
- [63] Rotondo P, Cosentino Lagomarsino M and Viola G 2015 *Phys. Rev. Lett.* **114** 143601
- [64] Hepp K and Lieb E H 1973 *Ann. Phys., NY* **76** 360
- [65] Wang Y K and Hioe F 1973 *Phys. Rev. A* **7** 831
- [66] Prokof'ev N, Svistunov B V and Tupitsyn I S 1998 *Phys. Lett. A* **238** 253
- [67] Prokof'ev N, Svistunov B V and Tupitsyn I S 1998 *J. Exp. Theor. Phys.* **87** 310
- [68] Ishino T, Saito R and Kamimura H 1990 *J. Phys. Soc. Japan.* **59** 3886
- [69] Hamermesh M 1962 *Group Theory and its Application to Physical Problems* (New York: Dover)
- [70] Ma Z-Q 2007 *Group Theory for Physicists* (Singapore: World Scientific)
- [71] Balasubramanian K 1985 *Chem. Rev.* **85** 599
- [72] Keller M and Trotter W 2014 *Applied Combinatorics* Preliminary edn <https://people.math.gatech.edu/~trotter/book.pdf>
- [73] Cameron P J 2008 *Introduction to Algebra* (Oxford: Oxford University Press)
- [74] Gallian J A 2006 *Contemporary Abstract Algebra* (Belmont, CA: Brooks/Cole, Cengage Learning)
- [75] Tannoudji C C, Dupont-Roc J and Grynberg G (ed) 1998 *Atom-Photon Interactions* (Weinheim: Wiley)
- [76] Emary C and Brandes T 2003 *Phys. Rev. E* **67** 066203
- [77] Dimer F, Estienne B, Parkins A S and Carmichael H J 2007 *Phys. Rev. A* **75** 013804